

This is the accepted manuscript made available via CHORUS. The article has been published as:

Cross section for the neutron radiative capture on ^{173}Lu nuclei

A. Ebran, O. Roig, V. Méot, M. Jandel, C. Theroine, E. M. Bond, T. A. Bredeweg, A. Couture, F. M. Nortier, J. M. O'Donnell, W. A. Taylor, J. L. Ullmann, and D. J. Vieira

Phys. Rev. C **99**, 064603 — Published 5 June 2019

DOI: [10.1103/PhysRevC.99.064603](https://doi.org/10.1103/PhysRevC.99.064603)

Cross section for the neutron radiative capture on ^{173}Lu nuclei

A. Ebran,¹ O. Roig,¹ V. Méot,¹ M. Jandel,² C. Theroine,¹ E. M. Bond,² T. A. Bredeweg,² A. Couture,² F. M. Nortier,² J. M. O'Donnell,² W. A. Taylor,² J. L. Ullmann,² and D. J. Vieira²

¹*CEA, DAM, DIF, F-91297 Arpajon, FRANCE*

²*Los Alamos National Laboratory, Los Alamos, New Mexico 87545, USA*

(Dated: April 15, 2019)

We report the measurement of a neutron radiative cross section on a target with a high gamma activity, at the Los Alamos DANCE detector (Detector for Advanced Neutron Capture Experiments) for the first time. The (n,γ) reaction properties of the unstable ^{173}Lu isotope were studied. Two experimental campaigns were needed to determine the $^{173}\text{Lu}(n,\gamma)$ cross section out. They were performed at the Los Alamos Neutron Science Center (LANSCE) spallation neutron source facility. To this end, two targets were produced from an Hf sample using successively proton irradiation and chemicals separations. They were composed of ^{173}Lu , ^{174}Lu and ^{175}Lu isotopes. The two measurements were conducted at two-year intervals taking advantage of the difference of the isotopic decay lifetimes in order to identify resonances from the $^{173}\text{Lu}(n,\gamma)$ and $^{174}\text{Lu}(n,\gamma)$ reactions. Just over one hundred new resonances were observed, and the majority of which come from the $^{173}\text{Lu}(n,\gamma)$ reaction. Only a few of them were assigned to the $^{174}\text{Lu}(n,\gamma)$ reaction. As regards the $^{173}\text{Lu}(n,\gamma)$ reaction, the radiative neutron capture cross section was determined over the energy range from thermal neutron up to a 200 eV. The parameters of resonances in the resolved resonance region were extracted with the SAMMY code while calculations with TALYS determined the capture cross section in the unresolved resonances region. At the keV region, we performed standard TALYS calculations as well as more others microscopic investigations by substituting the standard TALYS photon strength function by another one from QRPA models.

I. INTRODUCTION

Nuclear reaction models are adjusted on a set of typical known experimental data and then applied to compute, *e.g.*, cross sections for applications ranging from stellar modelling to the design of nuclear power reactors [1, 2]. As their results are tested against new measurements, their reliability can be gauged and the models are eventually refined. Neutron-induced reaction cross sections generally, and neutron capture cross sections in particular, are of specific interest due to their strong impact in astrophysics and nuclear reactor studies. Among the many open reaction channels, the radiative neutron capture is the most difficult to predict due to its large variations from one isotope to another. Moreover, when the neutron flux becomes high, several successive capture reactions can occur, leading to radioactive nuclei for which experimental data are very sparse preventing model adjustment. For such captures on radioactive nuclei, experiment facilities as nTOF at CERN or DANCE (Detector for Advanced Neutron Capture Experiment) at Los Alamos have been built. The lutetium isotopic chain is amenable to these types of measurements: ^{173}Lu ($t_{1/2}=1.37$ yr) and ^{174}Lu ($t_{1/2}=3.31$ yr) are relatively long-lived, making them candidates for target production. Recently, neutron capture cross sections for both stable isotopes, ^{175}Lu and ^{176}Lu , have been performed at the DANCE facility [16, 21] and comparison with the radiative neutron capture on the unstable ^{173}Lu and ^{174}Lu should provide useful information to examine the predictive capability of nuclear reaction models. The difficulty is now twofold, *viz.* *i)* make a pure unstable nuclei target and *ii)* perform measurements on such radioactive material. To this end, the ^{173}Lu target production as well as the cross section measurements were performed at the Los Alamos National Laboratory. The production of the ^{173}Lu sample used a novel method to isolate exclusively Lu isotopes: ^{173}Lu , ^{175}Lu and ^{174}Lu . The contribution from the $^{175}\text{Lu}(n,\gamma)$ reaction, well tabulated in the literature [3], was easily identified and was used as reference. However, two experiments, and so the fabrication of two targets, were necessary to separate the ^{173}Lu contribution from the ^{174}Lu one using differences in lifetime between the two isotopes. The two experiments were performed in December 2011 and in January 2014 using the DANCE array at flight path FP14 at the LANSCE-Lujan Center. In a first section the experimental set-up is introduced. Then we present the data analysis before discussing the results. The parameters of resonances for the resolved resonance region were calculated with the SAMMY code to well reproduce our experimental data. TALYS calculations were performed in order to determine the capture cross section in the unresolved resonance region. The calculation of the $^{173}\text{Lu}(n,\gamma)$ cross section will be achieved using the generalized lorentzian model for the gamma strength functions and Gilbert and Cameron formula for level densities. In this framework, gamma strength functions are normalized using the factor obtained with the well-known $^{175}\text{Lu}(n,\gamma)$ reaction. In order to improve the calculation we used a more microscopic approach using the QRPA (Quasiparticle Random Phase Approximation) formalism for the determination of the gamma strength functions and microscopic combinatorial model to get level densities. We will show that this approach allows reproduction of neutron capture cross section without any normalization.

II. EXPERIMENTAL CONSIDERATIONS

A. LANSCE facility and DANCE array

The ^{173}Lu radiative neutron capture cross section measurement was performed at the LANSCE (Los Alamos Neutron Science Center) facility [4]. A 800 MeV proton beam from the LANSCE linac accelerator is compressed into the proton storage ring (PSR) to a 250 ns pulse before impinging on a tungsten target with a 20 Hz repetition rate to produce fast neutrons [5]. The resulting neutrons are cooled down in a water moderator and collimated into flight path 14 (FP14) at the Manuel Lujan Jr. Neutron Scattering Center with an energy range from subthermal neutron up to 100 keV. The DANCE detector array is located at 20.25 m from the upper-tier water moderator.

This detector is an almost 4π γ -ray calorimeter made of 160 fast timing BaF_2 scintillation crystals surrounding a sample and designed for acquiring capture reactions data on small quantities of radioactive isotopes. The $\Omega = 3.95\pi$ large solide angle coverage of the detector and the high efficiency of BaF_2 crystals enable detection of a γ cascade with an efficiency above 95 % [6–10].

The maximal number of counts the DANCE detector can accept is expected to be around 3×10^7 γ /s/ 4π [11]. In order to optimize the signal to background ratio, we simulated the mass of each target consistently with the goals of both experiments, *i.e.* an accurate measurement of the maximal number of resonances during the first experiment and the identification of the first resonances in the second one. We estimated the detector response with respect to the various experimental conditions (target masses and shielding thickness) using GEANT4 to reproduce the DANCE detector responses [8, 12, 13]. GEANT4 simulations was fed by calculated γ -rays from the CEA/DAM EVITA Monte-Carlo code based on the Hauser-Feshbach formalism and able to reproduce a γ -cascade event from any nucleus involved in a capture reaction [16]. Level scheme and neutron transmission coefficients used as inputs by EVITA are computed with TALYS [1]. For the first experiment we run with a thick target to maximize the (n,γ) reactions. The latter

was surrounded by a Pb shielding in order to attenuate a large number of low energy γ -rays coming from the ^{173}Lu decay and hence to decrease its high counting rate to $3 \times 10^7 \gamma/\text{s}/4\pi$. The second experiment required less counting rate. Therefore a much smaller target was used in order to run without shielding, avoiding the significant associated deterioration of the detectors response.

B. Sample fabrication

Both samples were produced in the same way from a single stock solution. The stock solution was extracted of an irradiated Hf sample. This 49.12 g Hf sample was firstly irradiated into the Los-Alamos Isotope Production Facility (IPF) by 93 MeV energy proton beam from the LANSCE linac accelerator over a period of 14 days. During this irradiation, the dominant reaction is the (p,xn) reaction. It produced Ta isotopes ($^{173-174-175-176}\text{Ta}$) that decay into Hf then Lu isotopes. The (p,x α) reactions, with a smaller contribution, fed directly the production of Lu isotopes ($^{173-174-175}\text{Lu}$) (cf. Fig. 1). The sample was placed in a hot cell to cool for several months afterwards assuring that all shorter lived isotopes had decayed away. The lutetium isotopes, mainly produced by the β -decay of the tantalum isotopes, were next extracted from the Hf sample by a first chemistry separation in a mother solution. This mother solution was then split in two in order to produce two targets for both experiments. The daughter solutions were purified from lutetium β -decays products (Yb isotopes) and molecular plated onto a 2.5 μm thick high purity titanium foil by electrodeposition just after [14, 15] separation, in 2011 for the first target and in 2013 for the second one, just before undertaking the measurements. The target masses were determined from simulations to optimize the signal to background ratio.

The characterization of both targets was performed by optical emission spectroscopic analysis to determine the total lutetium mass and the $^{173,174}\text{Lu}$ activities were measured using the 272 keV and the 1241 keV γ -ray respectively. Specific masses of the main isotopes for both targets are reported Tab I.

^{173}Ta 3.14 h ϵ :100%	^{174}Ta 1.14 h ϵ :100%	^{175}Ta 10.5 h ϵ :100%	^{176}Ta 8.09 h ϵ :100%	^{177}Ta 56.6 h ϵ :100%	^{178}Ta 9.31 min ϵ :100%	^{179}Ta 1.82 yr ϵ :100%	^{180}Ta 8.15 h ϵ :100%	^{181}Ta STABLE 99.99%	- (p,xn) - (p,x α) - β -decay
^{172}Hf 1.87 yr ϵ :100%	^{173}Hf 23.6 h ϵ :100%	^{174}Hf 2.0×10^5 yr ϵ :100%	^{175}Hf 70 d ϵ :100%	^{176}Hf STABLE 5.26%	^{177}Hf STABLE 18.60%	^{178}Hf STABLE 27.28%	^{179}Hf STABLE 13.62%	^{180}Hf STABLE 35.08%	
^{171}Lu 8.24 d ϵ :100%	^{172}Lu 6.70 d ϵ :100%	^{173}Lu 1.37 yr ϵ :100%	^{174}Lu 3.31 yr ϵ :100%	^{175}Lu STABLE ϵ :100%	^{176}Lu 3.8×10^{10} yr 2.60% β :100%	^{177}Lu 6.65 d β :100%	^{178}Lu 28.4 min β :100%	^{179}Lu 4.59 h β :100%	
^{170}Yb STABLE 2.98%	^{171}Yb STABLE 14.09%	^{172}Yb STABLE 21.68%	^{173}Yb STABLE 16.10%	^{174}Yb STABLE 32.03%	^{175}Yb 4.19 d β :100%	^{176}Yb STABLE 2.98%	^{177}Yb 1.19 h β :100%	^{178}Yb 74 min β :100%	
^{169}Tm STABLE 100%	^{170}Tm 128.6 d ϵ :0.1% β :99.9%	^{171}Tm 1.92 yr β :100%	^{172}Tm 63.6 h β :100%	^{173}Tm 8.24 h β :100%	^{174}Tm 5.4 min β :100%	^{175}Tm 15.2 min β :100%	^{176}Tm 1.9 min β :100%	^{177}Tm 90 s β :100%	

FIG. 1: Production pathways for the main isotopes in the target.

Isotope	Half Life	Target produced in 2011			Target produced in 2013		
		Activity [mCi]	Activity [Bq]	Mass [μg]	Activity [mCi]	Activity [Bq]	Mass [μg]
^{173}Lu	1.37 years	79.01	2.92×10^9	52.39	1.32	4.9×10^7	3.84
^{174}Lu	3.3 years	1.9	0.07×10^9	3.06	0.02	6.7×10^5	0.31
^{175}Lu	-	-	-	166.05	-	-	5.85
Total Lu		80.91	2.99×10^9	221.5	1.34	4.97×10^7	10.0

TABLE I: Composition of both targets in 2011 and 2013.

A target mass of 52.39 μg of ^{173}Lu surrounded by a 9 mm thickness Pb liner was first used in the 2011 experiment which aimed at measuring the total capture cross section of the target. As for the identification of the first resonances in the 2013 experiment, a target with a smaller mass (3.84 μg) and without any need for shielding was enough.

C. DANCE Acquisition

The DANCE data acquisition (DAC) system is based on waveform digitization. Each BaF_2 photomultiplier output waveform is processed on-line by an Acqiris DC265 digitizer with 8-bit ADC resolution at a sampling rate of 500 MHz before extracting the main parameters which are then stored in 8-bit format on a disk (background baseline and fast and slow components of the light detector output).

The DAC, configured in so-called continuous mode, recorded data during two independent 250 μs wide time windows [17, 18]. During the experiment, one 250 μs wide window was dedicated at the keV energy region and pre-sample data¹. The second 250 μs wide window varied to scan the region from sub-eV to keV neutron energy.

Digitized signals were then read-out by the FARE (Fast reader) C++ code to reconstruct for each event the following critical values used during the data analysis, namely the time signal of each detector relative to the pulse signal, the total γ -ray cascade energy E_{sum} , the M_γ γ -multiplicity of each event and E_γ , the γ -ray energy of each crystal [13, 19].

III. DATA ANALYSIS

A. Calibration

The neutron flux ϕ_{Li} was monitored by Si detector viewing a ^6LiF foil located 2.5 m downstream the target position. The flux ϕ at the target position was calculated from the equation $\phi_{Li} = \alpha \times \phi$ by measuring the well-known 4.9 eV resonance of the $^{197}\text{Au}(n, \gamma)$ reaction to get the α factor. This factor includes the difference of the position between the beam monitor and the target as well as the unmeasured absolute $^6\text{Li-Si}$ efficiency. The neutron beam energy was determined by the time-of-flight technique.

A standard energy calibration with dedicated γ -sources was no longer possible due to the high activity rate target. The calibration was therefore performed using two γ -rays coming from the ^{173}Lu and ^{174}Lu isotopes decay, Tab. II and Fig. 2. In order to take into account the energy deviation over time of the detectors, we performed several energy calibration procedures during the experiments.

Isotope	E_γ [keV]	I_γ	Decay mode
^{173}Lu	636.1 ± 3	1.45 ± 5	e
^{174}Lu	1241.9 ± 6	5.14 ± 10	e + β^+

TABLE II: Lutetium isotope, energy, intensity and decay mode of γ -ray used for the energy calibration.

B. Background reduction

The most important background came from the decay of ^{173}Lu . This decay is expected to produce a low multiplicity ($M_\gamma < 3$) and low E_{sum} value ($E_{sum} < 4\text{MeV}$), and it was eliminated by selections on E_{sum} and M_γ , Tab. III. Thus, only the DANCE data for which the energy E_{sum} is between 4 MeV and 7 MeV and the multiplicity $M_\gamma < 3$ is between 3 and 8 are considered in the analysis. These cut selections have a significant impact on the signal to background

Isotope	Q value (MeV)	E_{sum} cut values (MeV)	M_γ cut values
^{173}Lu	6.760	[4, 7]	[3, 8]
^{174}Lu	7.666	[4, 7]	[3, 8]
^{175}Lu	6.300	[4, 7]	[3, 8]

TABLE III: Cut values applied on DANCE data to free from the main background noise.

¹ These data were recorded before the (n, γ) reactions included the γ -flash of the accelerator. They were useful to evaluate a part of the target background and to give a t_0 time useful to deduce the neutron energy. They are called pre-sample data.

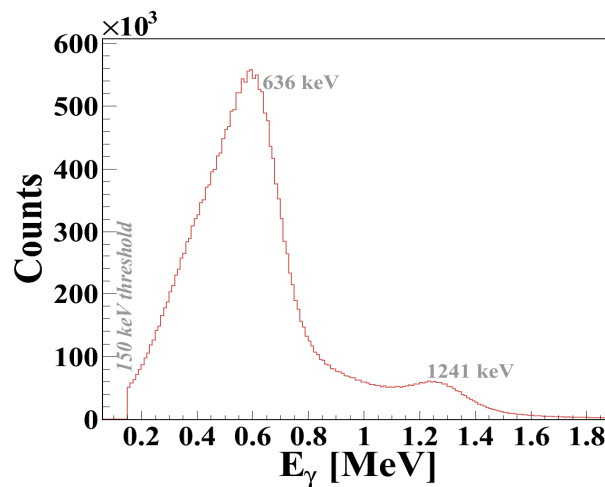


FIG. 2: 636 keV and 1241 keV γ -ray used for energy calibration from the energy spectrum of the BaF₂ crystal no 8.

ratio, Fig. 3. Radiodecay background suppression of $> 10^5$ was achieved with these cuts.

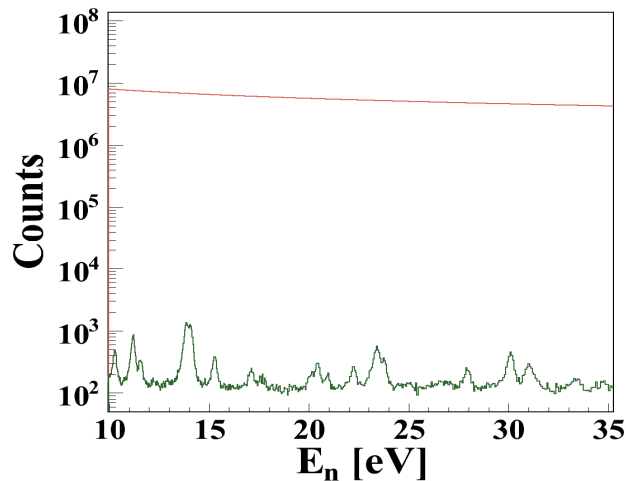


FIG. 3: Neutron energy spectrum with (black line) and without (red line) raw data reduction cuts. We can notice that for the raw data, the resonances are totally drowned in background but they b with cut selections.

C. Detection Efficiency

The γ -cascade detection efficiencies of ^{174}Lu and ^{176}Lu compound nuclei were obtained by comparison between the measured values and simulated data from the DANCE-GEANT4 code. By adding efficiencies from the $M_\gamma=3$ to higher, we found a γ -cascade detection efficiency of 4.15% for the ^{176}Lu compound nucleus and of 7.24% for the ^{174}Lu , Fig. 4. Such a variation comes from their different Q-values. At this stage, the contribution of the ^{175}Lu compound nucleus to the γ -cascades, expected to be low, was neglected.

IV. RESULTS AND DISCUSSION

The computation of the (n,γ) cross section on ^{173}Lu relies on the total capture yield that we extracted from our measurements. Besides ^{173}Lu , the latter also contained contributions from (n,γ) on ^{174}Lu and ^{175}Lu . Therefore, we

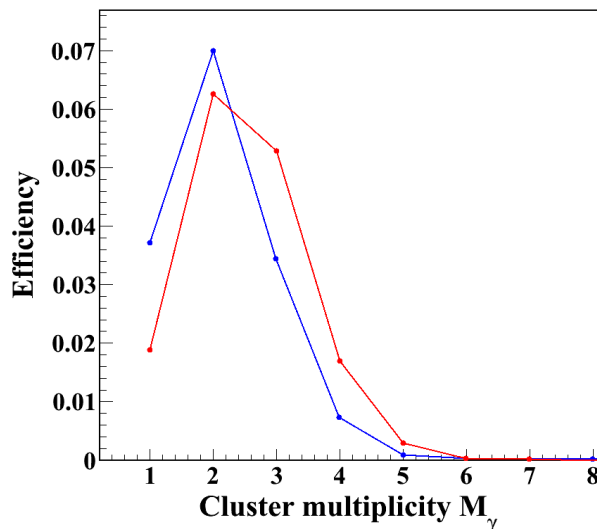


FIG. 4: Detection efficiency from EVITA DANCE-GEANT4 simulations for both $^{173}\text{Lu}(n,\gamma)$ and $^{175}\text{Lu}(n,\gamma)$ reactions.

first had to disentangle each contributions. Then, the resolved resonance region was analysed with the SAMMY code while we performed various calculations to tackle the unresolved resonance region with the TALYS code.

A. Total capture yield

The (n,γ) total capture yield $Y^{tot}(E_n)$ is defined for a given neutron energy E_n as the ratio of the total number of neutron capture events ($N_{n,\gamma}$) to the number of neutrons impinging the target (ϕ), Eq. (1).

$$Y^{tot}(E_n) = \frac{N_{(n,\gamma)}(E_n)}{\phi(E_n)} = Y^{^{173}\text{Lu}}(E_n) + Y^{^{174}\text{Lu}}(E_n) + Y^{^{175}\text{Lu}}(E_n) + Bck. \quad (1)$$

It was measured during the first experiment in December 2011 and is displayed in Fig. 5 over the neutron energy range from 2 eV to 2 keV.

B. Resonances identification

The total capture yield exhibits isolated resonances that can be associated to the $^{173}\text{Lu}(n,\gamma)$, the $^{174}\text{Lu}(n,\gamma)$ or the $^{175}\text{Lu}(n,\gamma)$ reactions. Since the $^{175}\text{Lu}(n,\gamma)$ reaction was previously investigated with the corresponding resonances referenced in the literature [3, 22, 25, 41], its contribution was the first to be identified. The remaining resonances were then assigned either to the $^{173}\text{Lu}(n,\gamma)$ or $^{174}\text{Lu}(n,\gamma)$ reactions. In order to disentangle their contributions, we took an advantage from different half-lives of the isotopes, namely $T_{1/2}^{^{173}\text{Lu}} = 1.37$ years and $T_{1/2}^{^{174}\text{Lu}} = 3.31$ years, motivating a second experiment to be conducted later. Measured under the very same conditions as the first experiment but two years later, the $^{173}\text{Lu}(n,\gamma)$ contribution was expected to decrease more than the $^{174}\text{Lu}(n,\gamma)$ one. Exploiting this property, we could identify each resonance up to 30 eV, *cf.* Fig. 6 where the total capture yields measured in 2011 (red line) and 2014 (black line) are compared. Decays of the ^{174}Lu , ^{175}Lu and ^{176}Lu compound nuclei are represented Fig. 7 by the blue, violet and black curves. The shadow areas represent 10% of error. For each identified resonances, we computed the corresponding number of counts from the total capture yields measured in 2014 and 2011. Their ratio $(\int_{\Delta E} \mathcal{R}es. dE)_{2014} / (\int_{\Delta E} \mathcal{R}es. dE)_{2011}$ is reported on the graphs by circles, stars and triangles for the $^{173}\text{Lu}(n,\gamma)$, $^{174}\text{Lu}(n,\gamma)$ and $^{175}\text{Lu}(n,\gamma)$ reactions. It allows identification of every resonances from 2 eV to 30 eV (*cf.* Tab. IV). As the identification uncertainty becoming too high due to the weak statistics of the 2014 experiment beyond this energy, and considering the initial quantity of ^{173}Lu and ^{174}Lu , all new resonances above 30 eV have been assigned to the $^{173}\text{Lu}(n,\gamma)$ reaction.

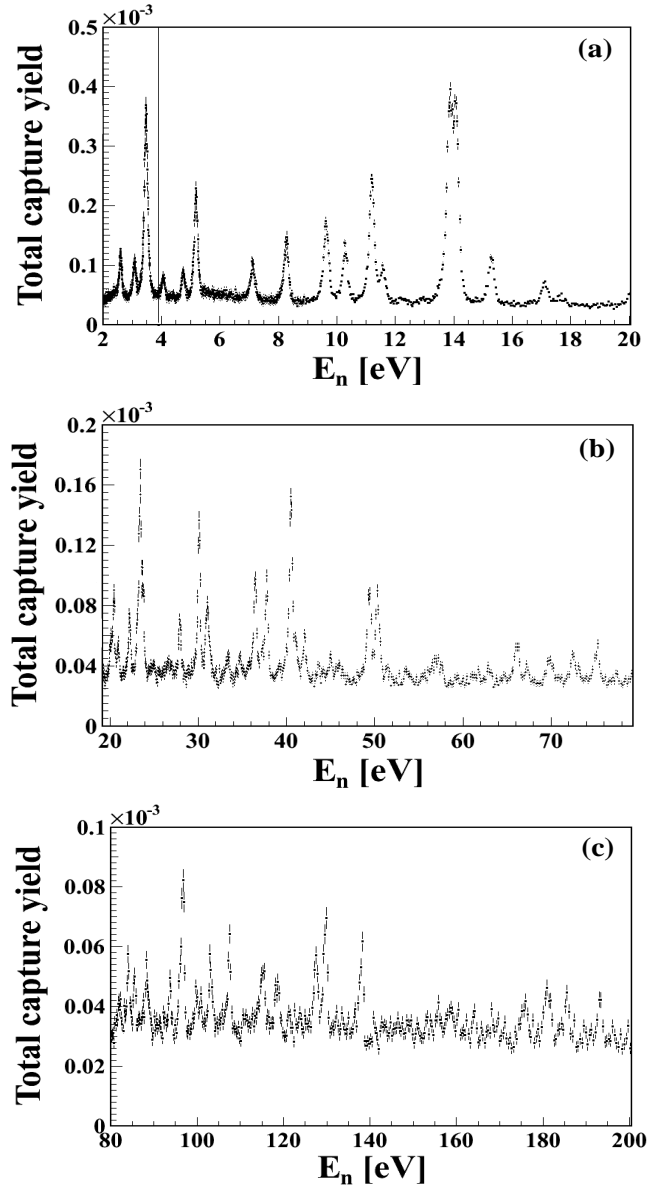


FIG. 5: Total capture yield with $3 < M_\gamma < 8$ and $4 \text{ MeV} < E_{\text{sum}} < 7 \text{ MeV}$ cut selections measured in December 2011 according to the incident neutron energy (a-c).

Up to 30 eV, we analysed 36 resonances, the 17.3 eV resonance displayed a too low statistics to be identified. Among the 35 remaining resonances, 11 were already known and came from the $^{175}\text{Lu}(n,\gamma)$ reaction, 18 have been assigned to the $^{173}\text{Lu}(n,\gamma)$ reaction and 6 to the $^{174}\text{Lu}(n,\gamma)$ reaction. Some new resonances overlapped strongly with $^{175}\text{Lu}(n,\gamma)$ ones, *e.g.* at $E_n=15.3 \text{ eV}$, 20.1 eV , 20.4 eV and 23.8 eV , making their identification challenging. We assign the first one to the $^{174}\text{Lu}(n,\gamma)$ reaction and the others to the $^{173}\text{Lu}(n,\gamma)$ reaction based on the values of the ratio $(\int_{\Delta E} \mathcal{R}es. dE)_{2014}/(\int_{\Delta E} \mathcal{R}es. dE)_{2011}$. Over all, 109 new resonances were assigned either to the $^{173}\text{Lu}(n,\gamma)$ or the $^{174}\text{Lu}(n,\gamma)$ reaction, thus bringing the number of resonances from $^{173}\text{Lu}(n,\gamma)$ to 103 and from $^{174}\text{Lu}(n,\gamma)$ to 6.

C. Resolved Resonance Region

The $^{173}\text{Lu}(n,\gamma)$ cross section and resonance parameters of the Resolved Resonance Region (RRR) were calculated with the R-matrix code SAMMY-7.0. The latter accounts for the Doppler broadening effects, the self-shielding and

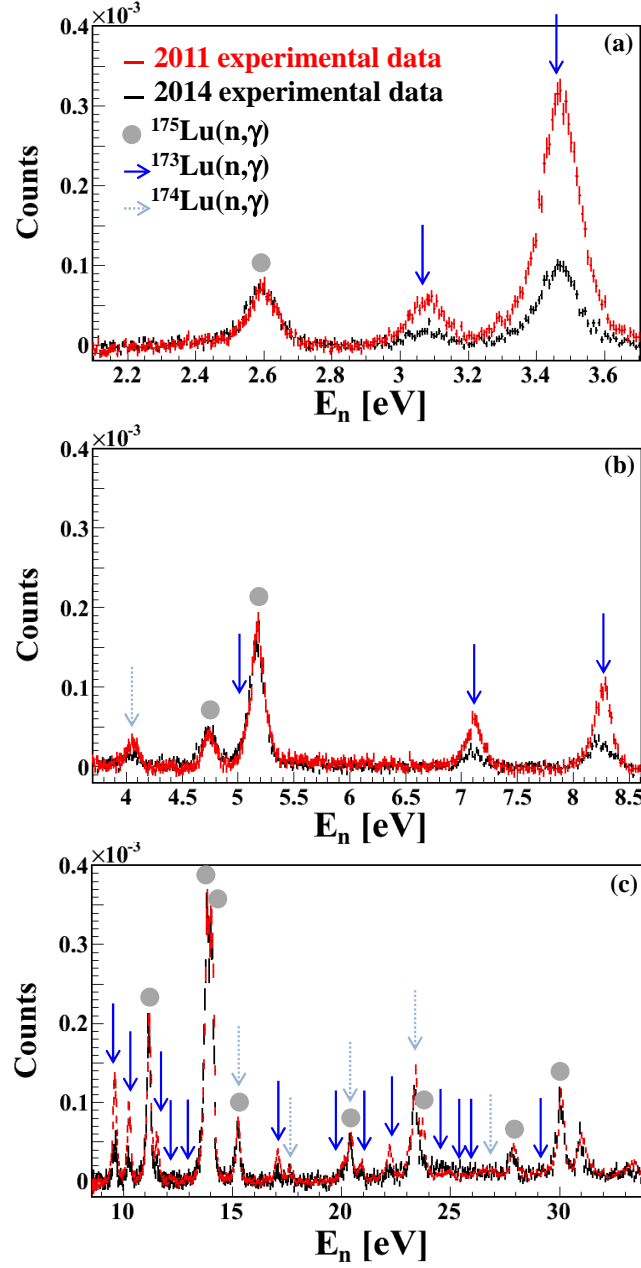


FIG. 6: Total capture yields from 2 eV to 30 eV (a-c) measured in 2011 (red line) and 2014 (black line). All resonances were assigned to the $^{175}\text{Lu}(n,\gamma)$, the $^{173}\text{Lu}(n,\gamma)$ or the $^{174}\text{Lu}(n,\gamma)$ reactions (circles, arrows and dashed arrows respectively).

the ToF resolution function facility by itself. Multiple scattering effects were considered as negligible because of the thickness of the target. About 100 new resonances were characterized. The consistency of the corresponding resonance parameters was checked using the SAMDIS module: a good agreement was found between the Γ_γ distribution and a χ^2 law, the average neutron widths are following a Porter-Thomas distribution [30] and the level spacing distribution follows a Wigner law, Fig. 8. Spin values of the ^{174}Lu compound nucleus levels were determined by the SUGGEL code [27] that computes the most probable value based on the $g\Gamma_n$, with g the spin statistical factor and Γ_n the neutron width. The SAMMY-7.0 cross section reconstruction of the $^{173}\text{Lu}(n,\gamma)$ reaction is displayed Fig. 9 and resonance parameters are listed in Tab. VII. From these characteristics, we deduce several parameters that are useful for constraining reaction models, namely :

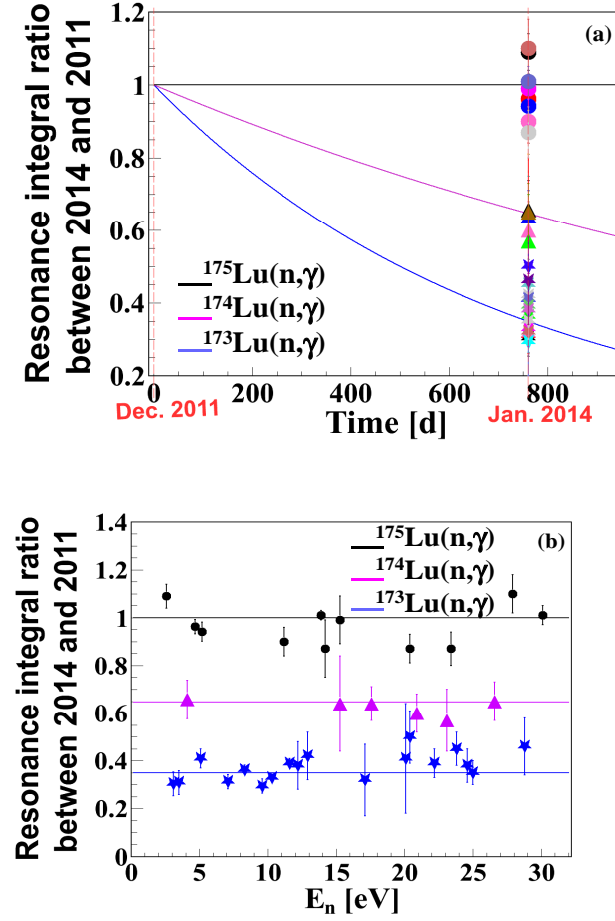


FIG. 7: (a) Resonance integrals ratio between 2014 and 2011 for $^{173-175}\text{Lu}(n,\gamma)$ reactions measured in December 2014 according to the decay of the different Lu isotopes. (b) Resonance integrals ratio between 2014 and 2011 for $^{173-175}\text{Lu}(n,\gamma)$ reactions according to the incident neutron energy.

1. The average gamma width, found to be $\langle \Gamma_\gamma \rangle = 73 \pm 2$ meV.
2. The orbital momentum l of each resonances, that we deduce using Eq. (2) [3]

$$\langle g\Gamma_n^l / \sqrt{E} \rangle = (2l + 1) V_l S_l D_l, \quad (2)$$

where the V_l , S_l and D_l parameters come as an output of the SAMMY code. The comparison between the corresponding values for s and p waves (red and blue lines respectively) and $\langle g\Gamma_n^l / \sqrt{E} \rangle$ extracted from the experimental data (black circles) is displayed in Fig. 10. All the experimental points are gathered around the theoretical value calculated for the s waves. Thereafter, we will assume that only s waves are seen up to 200 eV neutron energy, such that the average level spacing and the neutron strength function will now only be calculated for an orbital momentum $l=0$.

3. The average level spacing $\langle D_0 \rangle = \Delta E / N_0$ where the total number of levels N_0 ($N_0 \equiv N(x_l = 0)$) follows

$$N(x_{thr.}) = N_0 \int_{x_{thr.}}^{\infty} P_{PT}(x) dx = N_0 (1 - \text{erf} \sqrt{x_{thr.}/2}), \quad (3)$$

with $N(x_{thr.})$ the number of resonances such that the reduced neutron width is larger than a defined threshold $x_{thr.} = g\Gamma_{n,t}^0 / \langle g\Gamma_{n,t}^0 \rangle$, cf. Fig. 11. Extrapolating Eq. (3) to a null threshold yields $N_0 = 175$. Because 103 resonances were identified, it means that 72 other resonances were unresolved up to 200 eV. The average level spacing was calculated from the total N_0 value, that takes into account the observed and missing resonances, viz. $\langle D_0 \rangle = 1.15 \pm 0.33$ eV.

$^{173}\text{Lu}(n,\gamma)$		$^{174}\text{Lu}(n,\gamma)$		$^{175}\text{Lu}(n,\gamma)$	
E_n [eV]	Resonance Integral Ratio	E_n [eV]	Resonance Integral Ratio	E_n [eV]	Resonance Integral Ratio
3.1	0.30 ± 0.05	4.1	0.66 ± 0.08	2.6	1.09 ± 0.05
3.5	0.31 ± 0.05	15.3	0.64 ± 0.20	4.7	0.96 ± 0.03
5.1	0.41 ± 0.04	17.6	0.64 ± 0.07	5.2	0.94 ± 0.04
7.1	0.31 ± 0.03	20.9	0.60 ± 0.08	11.2	0.90 ± 0.06
8.3	0.36 ± 0.02	23.1	0.57 ± 0.13	13.9	1.01 ± 0.02
9.6	0.29 ± 0.03	26.6	0.65 ± 0.08	14.2	0.87 ± 0.12
10.3	0.33 ± 0.02			15.3	0.99 ± 0.10
11.6	0.39 ± 0.02			20.4	0.87 ± 0.06
12.2	0.38 ± 0.10			23.4	0.87 ± 0.07
12.9	0.42 ± 0.10			27.9	1.10 ± 0.08
17.1	0.32 ± 0.15			30.1	1.01 ± 0.04
20.1	0.41 ± 0.23				
20.4	0.50 ± 0.11				
22.2	0.39 ± 0.06				
23.8	0.45 ± 0.07				
24.6	0.38 ± 0.07				
25.0	0.35 ± 0.05				
28.8	0.46 ± 0.12				

TABLE IV: Identification of resonances up to 30 eV enabled by the difference of the lifetime of the lutetium isotopes.

4. The neutron strength function S_0 that can be extracted from the resonance characteristics according to

$$S_0 = \frac{\langle g\Gamma_n^0 \rangle}{\langle D_0 \rangle} = \frac{1}{\Delta E} \sum g\Gamma_n^0. \quad (4)$$

The cumulative sum of the reduced neutron width for every resonances as a function of neutron energy is plotted in the upper panel of Fig. 12 while the corresponding value of S_0 calculated at each neutron energy interval is displayed in the lower panel. Fitting according to a linear law (Eq. (4)) leads to the red line. Because of the high number of missed levels, data have been fitted from 2 eV to 80 eV leading to $S_0 = 1.6 \pm 0.3 \times 10^{-4}$.

D. Unresolved Resonance Region

The (n,γ) cross section of ^{173}Lu in the URR (Unresolved Resonance Region) was computed using the TALYS code. However, as no experimental data are available for this nucleus, ^{173}Lu , various calculations were achieved and compared to the better-known ^{175}Lu experimental case [25, 39, 40] in order to test them. The standard process allows TALYS to perform a normalization using the so-called G_{norm} factor. This G_{norm} factor takes into account the tabulated or given experimental data of the radiative width Γ_γ and level spacing D_0 as in the left member of the equation (5), and the calculated values as in the right member of the equation (5). The calculated values of Γ_γ and D_0 depends on the choice of the nuclear level density model, $\rho(S_n - E_\gamma, I', \Pi')$, and the γ strength function formalism, $f_{Xl}(E_\gamma)$. $f(X, \Pi', l)$ is related to the multipole selection rules.

$$\frac{2\pi\Gamma_\gamma}{D_0} = G_{norm} \sum_J \sum_{\Pi} \sum_{Xl} \sum_{I'=\lceil J-l \rceil}^{J+l} \sum_{\Pi'} \int_0^{S_n} 2\pi f_{Xl}(E_\gamma) E_\gamma^{2l+1} \rho(S_n - E_\gamma, I', \Pi') f(X, \Pi', l) dE_\gamma \quad (5)$$

In fact, this factor allows us to overcome the defects of the reaction model, to match experimental data and calculated values. The following results about evaluation would indicate the value of this G_{norm} factor. The G_{norm} factor could be also only adjusted in order to fit the cross section at the keV neutron energy region.

Thus, and because of the similarities of their proton number, spin structure, deformation and S_n value, we supposed that the nuclear structure of ^{173}Lu was close enough to the ^{175}Lu one to describe a compound formation process of the neutron capture on ^{173}Lu by using a ^{175}Lu adapted deformed Optical Model Potential (OMP) developed at CEA [26]. The corresponding neutron transmission coefficients were then obtained in the Hauser-Feshbach formalism. As for the γ -decay process of the compound nucleus, two key quantities drive its properties, *i.e.* the nuclear level density (NLD) and the γ (photon)-strength function (PSF). The gamma transmission coefficients, $T_{Xl}(E_\gamma) = 2\pi f_{Xl}(E_\gamma) E_\gamma^{2l+1}$ in Eq. (5), were obtained using the chosen PSF. As far as the NLD is concerned, the nuclear level scheme was taken

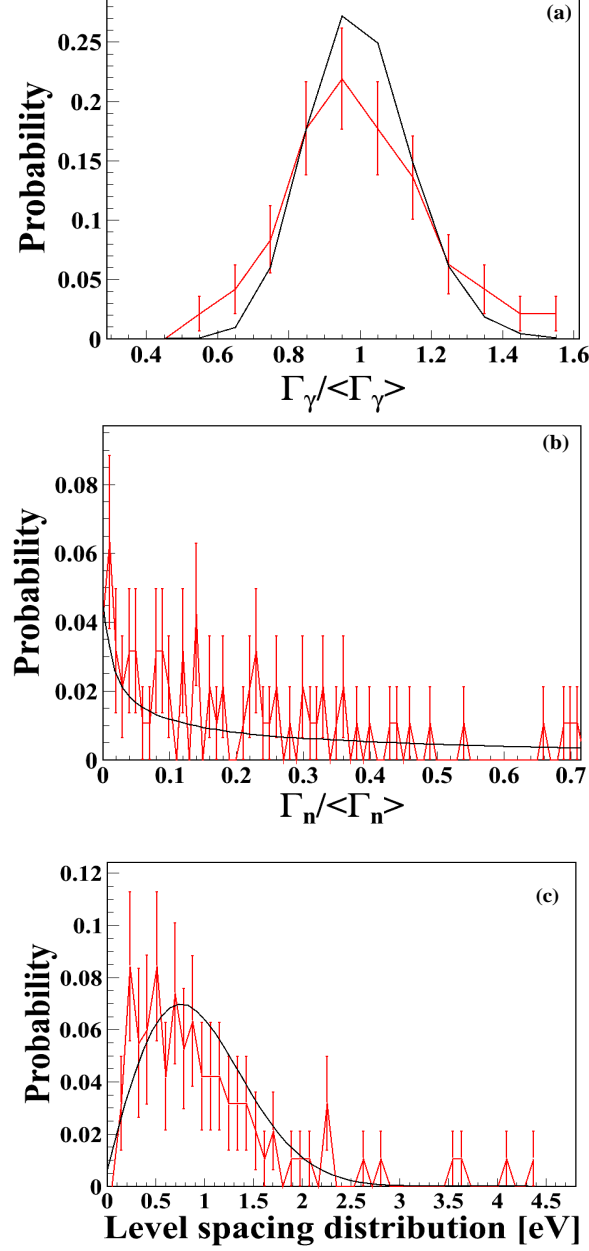


FIG. 8: Experimental data are represented by a red line while theoretical distributions are displayed in black.

(a) Reduced γ -width measured distributions compared to a χ^2 law ($\nu = 100$).

(b) Γ_n width compared to a Porter-Thomas distribution.

(c) Resonance spacings and Wigner distribution comparison.

from the RIPL-3 nuclear data library [32] and the corresponding NLD was obtained using the Gilbert and Cameron formula [33]. As the first step we focused on the $^{175}\text{Lu}(n,\gamma)$ reaction and we retained the first 56 discrete levels above the ground state to describe the ^{176}Lu compound nucleus. Regarding the PSF, we first worked within the phenomenological Generalized Lorentzian model (GLO model) of Kopecky-Uhl [34] for E1 transitions and within the Brink-Axel model (SLO model) [35] for M1 transitions.

Under these conditions, we found a G_{norm} value 2.3 to well reproduce the existing data at the keV region as it is shown on the Fig. 13.

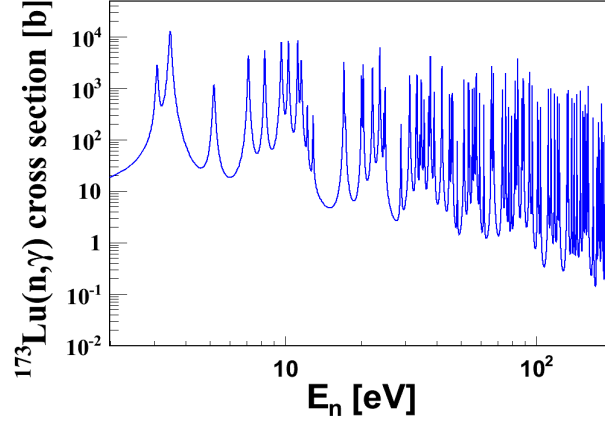


FIG. 9: $^{173}\text{Lu}(n,\gamma)$ reaction neutron cross section from the SAMMY-7.0 code over the resonance domain.

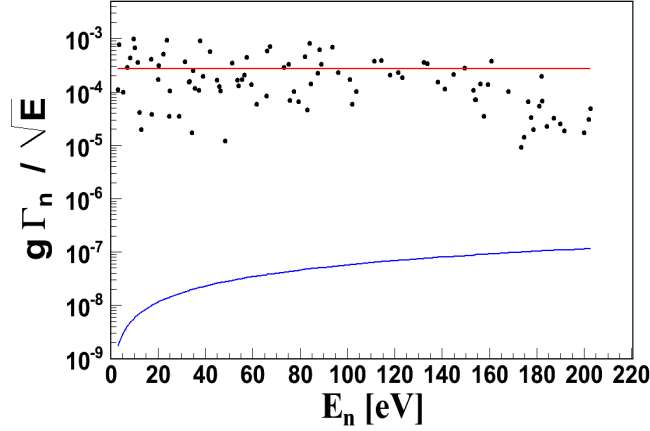


FIG. 10: Orbital momentum assignment of resonances.

To improve this calculation, we then went further working with a more microscopic NLD model, the microscopic level densities model from Hilaire-Goriely combinatorial tables using Skyrme forces [38] and with QRPA-based PSFs [43]. With a $G_{norm}=1$, the radiative capture, $^{175}\text{Lu}(n,\gamma)$, cross section matches well the experimental data from [25, 39, 40] in Fig. 13). Calculated values of $\Gamma_\gamma \times G_{norm}/D_0$ are compatible with the experimental one in the table V. This result makes us confident about calculating the radiative capture cross section of the $^{173}\text{Lu}(n,\gamma)$ reaction with a microscopic level density model and the QRPA-based PSFs. We retained the first 46 discrete levels above the ground state to describe the ^{174}Lu compound nucleus. The different parameters values are reported in the table VI.

The radiative capture, $^{173}\text{Lu}(n,\gamma)$, cross section is plotted in Fig. 14. The normalization method, one using results on ^{175}Lu , $G_{norm}=2.3$ in the keV neutron energy region, give results far from the experimental values in Table VI. Parameters are not compatible in 1σ standard uncertainty with the experimental data obtained in this work. The calculation using the microscopic models (NLD and QRPA PSFs) gives better results, compatible in 1σ standard uncertainty with the experimental data in Table VI. In Fig. 14, at keV neutron energy range, 17% and 35% differences are observed between both cross section normalizations at 1 keV and 100 keV respectively. Finally, the most confident radiative capture cross section for the reaction $^{173}\text{Lu}(n,\gamma)$ should be the most microscopic calculations (curve red in Fig. 14).

Indeed, we aim at well-calculating neutron radiative capture cross sections on nuclei for which no experimental data are available, which implies that we focus on more and more microscopic approaches to circumvent this issue.

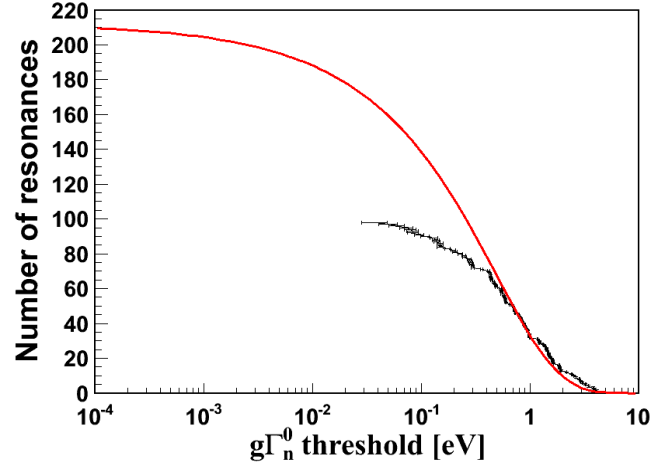


FIG. 11: Number of observed resonances with neutron widths larger than a threshold fitted by Eq. (3).

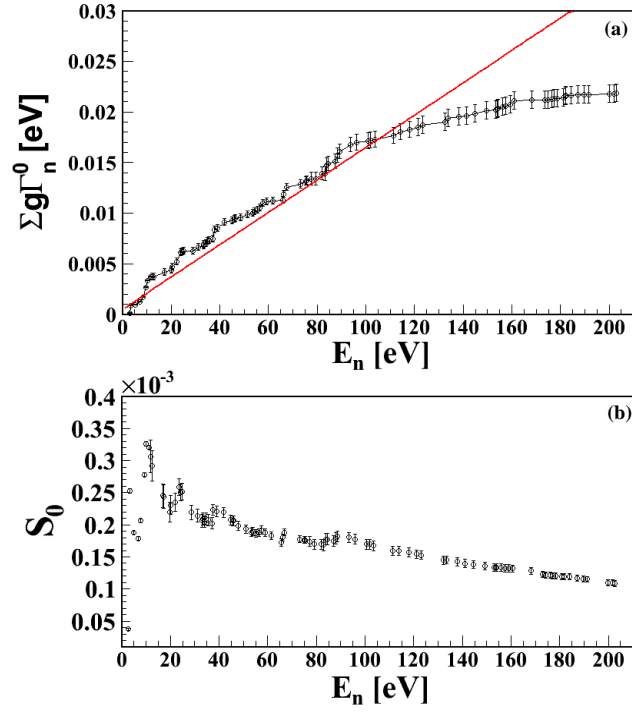


FIG. 12: (a) Cumulative sum of the reduced neutron widths as a function of the neutron energy. (b) Neutron strength function versus neutron energy.

V. CONCLUSION

For the first time a neutron capture cross section was measured and analyzed for a high γ -activity target. The $^{173}\text{Lu}(n,\gamma)$ cross section measurement was achieved at the Manuel Lujan Jr. Neutron Center using the DANCE array. Two experiments were necessary to determine and isolate the neutron capture cross section on ^{173}Lu from the ^{174}Lu contribution. We observed 109 new resonances up to 200 eV. Among them, 6 come from the ^{175}Lu compound nucleus and 103 were assigned to the $^{173}\text{Lu}(n,\gamma)$ reaction. Spin, Γ_γ and Γ_n were characterized for each of the 103 resonances by the SAMMY code and their consistencies were checked. Important parameters for the ^{174}Lu compound nucleus and useful to constrain theoretical models were extracted from these values, *i.e.* $\langle\Gamma_\gamma\rangle = 73 \pm 2$ meV, orbital

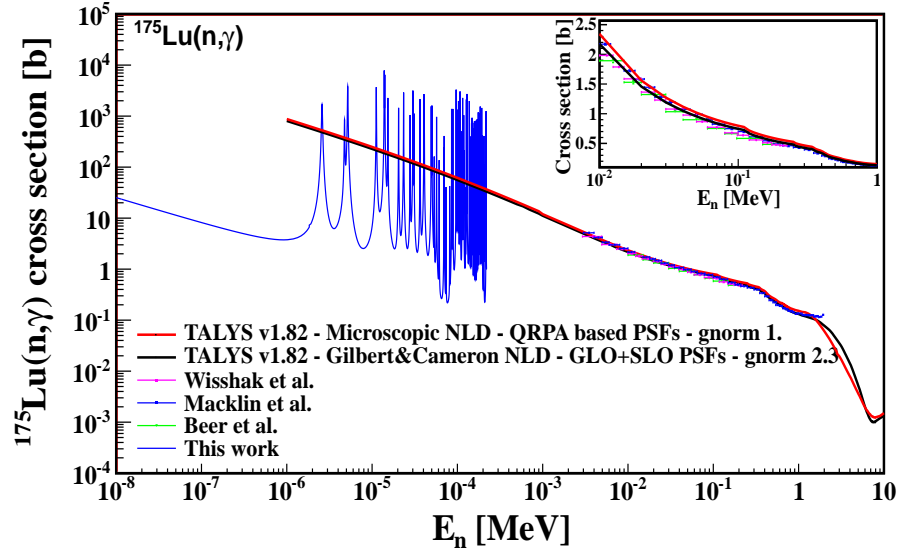


FIG. 13: Radiative capture cross section for $^{175}\text{Lu}(n,\gamma)$ reaction. Data from K. Wisshak [25] are plotted in pink, data from H. Beer [40] are in green and data from R.L. Macklin [39] are in blue. Standard TALYS calculation normalized at keV region is in black. Calculation computed with a E1, M1 PSFs from QRPA models is in red full lines.

TABLE V: ^{176}Lu Parameters calculated using the TALYS code or from the experimental data for the reaction $^{175}\text{Lu}(n,\gamma)$.

Parameters	Exp. [3]	Norm. at keV	QRPA based PSFs
G_{norm}	-	2.3	1.0
Γ_γ	77 ± 5 meV	24 meV	53 meV
S_0	$(1.82 \pm 0.12) \times 10^{-4}$	2.06×10^{-4}	2.06×10^{-4}
D_0	3.45 ± 0.15 eV	3.0 eV	2.53 eV
$\Gamma_\gamma \times G_{norm} / D_0$	0.022 ± 0.002	0.018	0.021

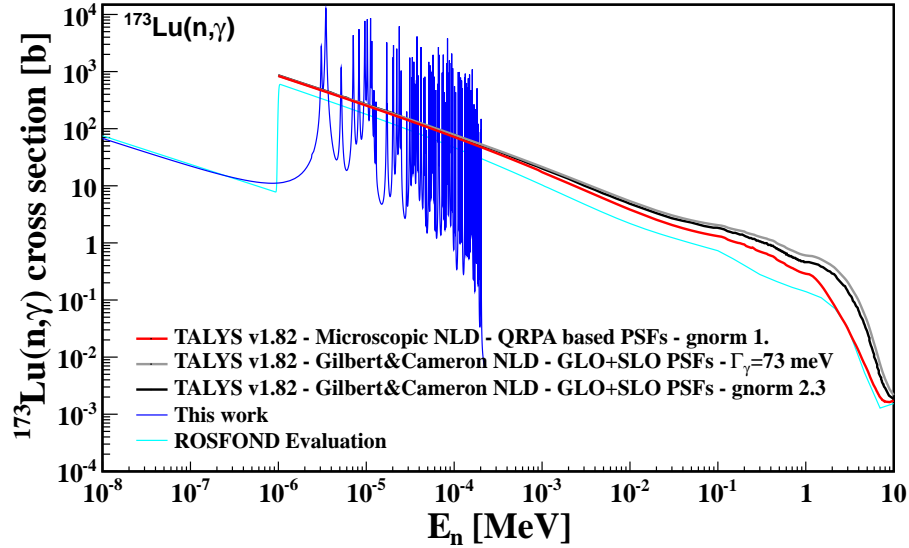


FIG. 14: Radiative capture cross section for $^{173}\text{Lu}(n,\gamma)$ reaction. Standard TALYS normalized calculations are in black curve for ^{175}Lu normalization ($G_{norm}=2.3$) and in grey curve for normalization based on experimental data from this work ($\Gamma_\gamma=73$ meV). Calculation computed with a E1, M1 PSFs from QRPA formalism is in red full line.

momentum assignment of resonances ($l=0$), $\langle D_0 \rangle = 1.15 \pm 0.33$ eV and $S_0 = (1.6 \pm 0.3) \times 10^{-4}$. We extended this study

TABLE VI: ^{174}Lu Parameters calculated using the TALYS code or from the experimental data for the reaction $^{173}\text{Lu}(n,\gamma)$.

Parameters	Exp. - <i>this work</i>	Norm. at keV	QRPA based PSFs
G_{norm}	-	2.3 (as ^{176}Lu)	1.0
Γ_γ	73 ± 15 meV	23 meV	79 meV
S_0	$(1.6 \pm 0.3) \times 10^{-4}$	2.06×10^{-4}	2.06×10^{-4}
D_0	1.15 ± 0.33 eV	0.58 eV	1.37 eV
$\Gamma_\gamma \times G_{norm} / D_0$	0.063 ± 0.022	0.091	0.058

to the unresolved resonance region with standard TALYS calculations that we improved by substituting the GLO model PSF of the latter by a microscopic E1 PSF from QRPA models using a microscopic NLD model. The latter method provides a very good result for the value of the average γ -width and reliable neutron capture cross section. This first high gamma activity target experiment proves the feasibility of such measurements and paves the way to a large campaign of radioactive sample studies.

VI. ACKNOWLEDGMENTS

This work was performed under the auspices of an agreement between CEA/DAM and NNSA/DP on cooperation on fundamental science. It has benefited from the use of the LANSCE facility at the Los Alamos National Laboratory, and was performed thanks to the US Department of Energy, National Nuclear Security Administration, by Los Alamos National Security, LLC, under Contract No. DE-AC52-06NA25396.

-
- [1] A.J. Koning *et al.*, Modern Nuclear Data Evaluation with the TALYS Code System, Nucl. Data Sheets **113**, 2841-2934 (2012).
- [2] C. Vockenhuber *et al.*, Stellar (n, γ) cross section of ^{174}Hf and radioactive ^{182}Hf , Phys. Rev. C **75**, 015804:1-14 (2007).
- [3] S.F. Mughabghab, Atlas Of Neutron Resonances, Resonance Parameters And Neutrons Cross Sections Z=1-100, Elsevier (2006).
- [4] P.W. Lisowski *et al.*, The Los Alamos Neutron Science Center, Nucl. Instr. & Meth. A **562**, 910-914 (2006).
- [5] P.W. Lisowski *et al.*, The Los Alamos National Laboratory Spallation Neutron Sources, Nucl. Sci. Eng. **106**, **208** (1990).
- [6] <http://geant4.cern.ch/>
- [7] E.I. Esch *et al.*, Measurement of the $^{237}\text{Np}(n,\gamma)$ cross section from 20 meV to 500 keV with a high efficiency, highly segmented 4π BaF₂ detector, Phys.Rev.C **77**, 034309:1-10 (2008).
- [8] M. Jandel *et al.*, Geant4 simulations of the DANCE array, Nucl. Instrum. Methods Phys. Res. B **261**, 1117-1121 (2007).
- [9] M. Heil *et al.*, A 4π BaF₂ detector for (n, γ) cross-section measurements at a spallation neutron source, Nucl. Instr. & Meth. A **459**, 229-246 (2001).
- [10] R. Reifarh *et al.*, Background identification and suppression for the measurement of (n, γ) reactions with the DANCE array at LANSCE, Nucl. Instrum. Methods Phys. Res. A **531**, 530-543 (2004).
- [11] A. Couture *et al.*, Direct measurements of neutron capture on radioactive isotopes, At. Data Nucl. Data Tables **93**, 807-830 (2007).
- [12] S. Agostinelli *et al.*, GEANT4-a simulation toolkit, Nucl. Instr. & Meth. A **506**, 230-303 (2003).
- [13] O. Roig *et al.*, Measurement of $^{173}\text{Lu}(n,\gamma)$ Cross Sections at DANCE, Nucl. Data Sheets **119**, 165-168 (2014).
- [14] W.A. Taylor *et al.*, Production of a ^{173}Lu target for neutron capture cross section measurements, J. Radioanal Nucl. Chem. **282**, 391-394 (2009).
- [15] W.A. Taylor *et al.*, Recent developments in the manufacture of ^{173}Lu targets, J. Radioanal Nucl. Chem. **296**, 689-692 (2013).
- [16] D. Denis-Petit, Isomeric ratio measurements for the radiative neutron capture $^{176}\text{Lu}(n,\gamma)$ at the LANL DANCE facility, Phys. Rev. C **94**, 054612:1-12 (2016).
- [17] J.M. Woutes *et al.*, Acquisition-Analysis System for the DANCE (Detector for Advanced Neutron Capture Experiment) BaF₂ Gamma-Ray Calorimeter, IEEE Transaction on Nucl. Sc. **53**, 00018-9499 (2006).
- [18] M. Jandel *et al.*, Neutron capture cross section of ^{241}Am , Phys. Rev. C **78**, 034609:1-15 (2008).
- [19] M. Jandel and Todd A. Bredeweg and A. Couture and J. M. O'Donnell and J. L. Ullmann, FARE - software for DANCE data analysis, Los Alamos National Lab., LANL Reports, LA-UR-12-21171 (2012)
- [20] D.D. Vieira *et al.*, Neutron Capture and (n,2n) Measurements on ^{241}Am , Intern. Conf. on Nucl. Data for Sc. and Techn., UCRL-CONF-232955 (2007).
- [21] O. Roig *et al.*, Radiative neutron capture cross section on ^{176}Lu at DANCE, Phys. Rev. C **93**, 034602:1-11 (2016).
- [22] H. Beer *et al.*, Neutron capture cross sections and solar abundances of $^{160,161}\text{Dy}$, $^{170,171}\text{Yb}$, $^{175,176}\text{Lu}$ and $^{176,177}\text{Hf}$ for the s-process analysis of the radionuclide ^{176}Lu , Phys. Rev. C **30**, 464-478 (1984)
- [23] R.L. Macklin and D.M. Drake and J.J. Malanify, Fast Neutron Capture Cross Sections of ^{169}Tm , ^{191}Ir , ^{193}Ir , and ^{175}Lu for $3j=E(n)=2000$ keV., Los Alamos Scientific Lab. Reports, No.7479, p.MS (1978)
- [24] M. V. Bokhovko *et al.*, Obninsk Reports FEI 2169, Fiziko Energeticheskij Institut (1991).
- [25] K. Wisshak *et al.*, Stellar neutron capture cross sections of the Lu isotopes, Phys. Rev. C **73**, 015807:1-10 (2006).
- [26] P. Romain *et al.*, PROC. SPECIALISTS MEETING ON THE NUCLEON-NUCLEUS OPTICAL MODEL UP TO 200 MEV, 167, <http://db.nea.fr/html/science/om200> (1997).
- [27] S. Oh *et al.*, ORNL/TM- 2000-314, Oak Ridge National Laboratory (2001), <https://www.osti.gov/scitech/biblio/777661>.
- [28] F.J. Dyson *et al.*, Statistical Theory of the Energy Levels of Complex Systems.IV, J. Math. Phys. **4**, 701-712 (1963).
- [29] E.P. Wigner, Results and theory of resonance absorption, Conf. on Neutron Phys. by time-of-flight, Report ORNL 2309 (1956).
- [30] C.E. Porter, Fluctuations of Nuclear Reaction Widths, Phys. Rev. **104**, 483-491 (1956).
- [31] A.J. Koning *et al.*, TALYS-1.0: A nuclear reaction program, User Manual, www.talys.eu. ^{173}Lu and ^{174}Lu
- [32] R. Capote *et al.*, RIPL - Reference Input Parameter Library for Calculation of Nuclear Reactions and Nuclear Data Evaluations, Nucl. Data Sheets **110**, 3107-3214 (2009).
- [33] A. Gilbert and A. G. W. Cameron, A composite nuclear-level density formula with shell corrections, Can. J. Phys. **43**, 1446-1496 (1965).
- [34] J. Kopecky *et al.*, Radiative strength in the compound nucleus ^{157}Gd , Phys. Rev. C **47**, 312-322 (1993).
- [35] D. M. Brink, Ph.D. thesis, Oxford University, 1955 (unpublished).
- [36] M. R. Mumpower *et al.*, Estimation of M1 scissors mode strength for deformed nuclei in the medium- to heavy-mass region by statistical Hauser-Feshbach model calculations, Phys. Rev. C **96**, 024612:1-10 (2017).
- [37] J.L. Ullmann *et al.*, Cross section and γ -ray spectra for $^{238}\text{U}(n,\gamma)$ measured with the DANCE detector array at the Los Alamos Neutron Science Center, Phys. Rev. C **89**, 034603:1-8 (2014).
- [38] S. Hilaire *et al.*, Potential sources of uncertainties in nuclear reaction modeling, European Journal of Physics N, *to be published*.
- [39] R.L. Macklin *et al.*, Fast Neutron Capture Cross Sections of ^{169}Tm , ^{191}Ir , ^{193}Ir , and ^{175}Lu for $E_n=2000$ keV, Technical report **7479**, 1978. Los Alamos Scientific Lab. Reports.

- [40] H. Beer *et al.*, Lu-176 Cosmic clock or stellar thermometer, *Astrophysical Journal, Supplement* **46**, 295 (1981)
- [41] M.V. Bokhovko *et al.*, Neutron radiation capture cross-section and transmission of fast neutrons for nuclei of rare-earth elements Ta-181 and Os-187, *Fiz.-Energ Institut, Obninsk Reports*, No.2169, p.91 (1991), Russia
- [42] M. Martini *et al.*, Large-scale deformed quasiparticle random-phase approximation calculations of the γ -ray strength function using the Gogny force, *Phys.Rev.C* **94**, 014304:1-15 (2016).
- [43] S. Goriely *et al.*, Gogny-Hartree-Fock-Bogolyubov plus quasiparticle random-phase approximation predictions of the M1 strength function and its impact on radiative neutron capture cross section, *Phys.Rev.C* **94**, 044306:1-9 (2016).
- [44] J. Kopecky *et al.*, E1 and M1 strength functions from average resonance capture data, *Phys.Rev.C* **95**, 054317:1-11 (2017).

J	Energy (eV)	Γ_γ (meV)	Γ_n (meV)
3	3.1 (2)	62 (8)	0.44 (0.02)
3	3.5 (7)	77 (8)	3.25 (0.05)
4	5.1 (7)	77 (8)	3.25 (0.05)
3	7.1 (3)	81 (7)	1.75 (0.08)
4	8.3 (2)	67 (9)	2.87 (0.13)
3	9.6 (2)	93 (8)	6.89 (0.12)
3	10.3 (4)	76 (9)	4.90 (0.09)
4	11.6 (5)	93 (13)	2.51 (2.43)
4	12.2 (7)	71 (7)	0.33 (0.19)
4	12.9 (7)	65 (6)	0.16 (0.07)
3	17.1 (2)	91 (11)	4.16 (0.15)
4	17.3 (5)	114 (51)	2.81 (0.78)
4	20.1 (5)	71 (6)	1.75 (0.22)
3	20.4 (7)	56 (8)	3.19 (0.27)
3	22.2 (5)	102 (36)	5.49 (0.38)
4	23.8 (3)	82 (16)	10.33 (0.41)
4	24.6 (5)	78 (17)	0.40 (0.44)
3	25.0 (8)	66 (29)	1.19 (0.41)
3	28.8 (6)	87 (32)	0.43 (0.73)
3	31.3 (2)	77 (28)	4.50 (0.61)
4	33.4 (5)	48 (26)	1.63 (0.42)
4	34.2 (2)	72 (11)	1.79 (0.56)
4	34.8 (2)	80 (65)	3.05 (0.75)
4	35.7 (7)	105 (94)	1.57 (0.60)
4	37.2 (4)	85 (76)	1.51 (0.21)
3	37.8 (9)	66 (59)	12.64 (0.53)
4	39.1 (1)	92 (72)	2.82 (0.47)
3	42.0 (5)	93 (49)	8.41 (0.55)
4	45.0 (4)	80 (28)	2.57 (0.54)
4	45.9 (6)	80 (13)	1.94 (0.68)
4	46.4 (4)	61 (41)	1.62 (0.79)
3	51.4 (11)	75 (29)	5.72 (0.58)
4	53.6 (6)	41 (21)	2.74 (0.14)
3	54.0 (4)	60 (36)	2.17 (1.12)
4	55.5 (9)	74 (39)	2.91 (1.03)
4	56.5 (11)	83 (41)	3.55 (0.72)
4	57.6 (6)	84 (32)	7.62 (0.66)
3	59.3 (9)	53 (43)	2.41 (0.87)
3	61.7 (7)	51 (38)	1.05 (1.21)
4	65.8 (5)	56 (37)	1.57 (0.90)
4	66.2 (1)	47 (28)	11.00 (0.81)
4	67.3 (2)	88 (37)	13.40 (1.46)
4	73.1 (4)	107 (62)	5.58 (9.35)
3	75.2 (3)	52 (36)	6.57 (3.55)
4	75.6 (2)	74 (19)	1.38 (2.11)
4	77.5 (1)	65 (29)	2.02 (6.68)
3	79.4 (7)	64 (31)	1.32 (1.16)
3	82.1 (9)	74 (20)	9.40 (1.57)
4	83.1 (9)	70 (55)	0.97 (1.34)
4	84.0 (2)	37 (33)	17.00 (3.10)
3	84.6 (3)	49 (33)	3.00 (0.85)
3	87.4 (7)	90 (32)	4.83 (2.90)
3	88.3 (9)	83 (29)	13.40 (2.42)
3	89.1 (1)	70 (58)	7.18 (2.82)
4	93.7 (7)	82 (32)	15.10 (0.98)
4	96.2 (2)	59 (40)	5.22 (2.18)

J	Energy (eV)	Γ_γ (meV)	$2g\Gamma_n$ (meV)
3	101.0 (8)	73 (31)	3.93 (3.96)
4	102.0 (2)	79 (51)	1.34 (4.46)
4	103.8 (1)	73 (40)	2.36 (3.43)
3	111.4 (1)	76 (42)	8.98 (3.17)
4	114.2 (1)	77 (39)	9.46 (2.13)
3	118.1 (3)	71 (42)	5.10 (3.38)
4	121.4 (2)	67 (47)	5.80 (2.79)
4	123.3 (2)	102 (91)	4.70 (1.96)
3	132.4 (2)	83 (40)	9.30 (1.99)
3	133.8 (2)	65 (58)	9.00 (0.98)
4	138.1 (2)	62 (32)	4.12 (0.23)
3	141.3 (2)	56 (34)	3.09 (0.37)
4	144.8 (2)	67 (37)	5.92 (1.91)
3	149.6 (2)	70 (47)	7.76 (0.93)
3	153.2 (1)	59 (51)	5.27 (0.53)
4	153.9 (2)	72 (64)	3.68 (1.63)
4	154.3 (2)	66 (59)	2.00 (2.71)
4	156.2 (2)	72 (74)	4.00 (0.64)
4	157.6 (2)	77 (69)	1.00 (0.98)
3	159.3 (2)	81 (32)	4.00 (0.72)
4	160.8 (2)	69 (28)	11.00 (0.53)
4	168.1 (2)	93 (39)	3.00 (0.51)
4	173.5 (2)	82 (43)	0.27 (0.91)
3	174.7 (2)	77 (41)	0.43 (1.42)
3	176.4 (2)	72 (28)	2.00 (0.37)
4	177.5 (2)	73 (41)	1.00 (1.91)
4	178.6 (2)	79 (36)	0.61 (0.93)
4	181.2 (2)	81 (48)	1.65 (0.53)
4	182.0 (2)	63 (43)	6.00 (1.63)
4	182.2 (2)	76 (35)	2.10 (2.71)
4	184.2 (2)	61 (38)	0.70 (0.64)
4	187.3 (2)	63 (57)	1.00 (0.98)
3	189.8 (5)	70 (49)	0.80(0.72)
3	191.5 (5)	69 (46)	0.59 (0.53)
3	200.0 (5)	62 (53)	0.56 (0.51)
4	201.9 (5)	56 (54)	1.00 (0.91)
4	202.8 (5)	57 (51)	1.57 (1.42)

TABLE VII: List of the 103 resonances assigned to the $^{173}\text{Lu}(n,\gamma)$ reaction up to 200 eV neutron energy and their parameters calculated with the SAMMY-7.0 code.